High-pressure effects on crystal structure and critical temperature in superconducting NbB_2 and stabilized MoB_2

*Kazuki Yamane[1,2], *Ryo Matsumoto[1], Takafumi D. Yamamoto[3], Kensei Terashima[1], Shintaro Adachi[4], Hiroyuki Takeya[5], Mitsuharu Nagasawa[6], Yoshihiko Takano[1,2]*

[1] Research Center for Materials Nanoarchitectonics (MANA), National Institute for Materials Science, Tsukuba, Ibaraki 305-0047, Japan

[2]Graduate School of Pure and Applied Sciences, University of Tsukuba, 1-1-1 Tennodai, Tsukuba, Ibaraki 305-8577, Japan

[3] Department of Material Science and Technology, Tokyo University of Science, Tokyo 125-8585, Japan

[4]Department of Mechanical and Electrical Systems Engineering, Faculty of Engineering, Kyoto University of Advanced Science (KUAS), Kyoto, 615-8577, Japan

[5] Research Center for Energy and Environmental Materials (GREEN) *National Institute for Materials Science, Tsukuba, Ibaraki 305-0047, Japan*

[6] Department of Natural Sciences, Tokyo Denki University, Adachi, Tokyo 120-8551, Japan

**Corresponding author; Email: MATSUMOTO.Ryo@nims.go.jp*

Abstract

Exploration for superconducting metal diborides with a high critical temperature (T_c) has attracted much attention since the discovery of MgB_2. Recently reported high T_c in compressed MoB_2 has motivated us to investigate the electrical transport property under high pressure in other metal diborides. We focused on the relationship between T_c and a stretched *c*-lattice parameter (*c*/*a*), known as an important parameter for superconductivity in MgB_2, which shows the main contribution of *p* electron to electronic structure. In this study, the correlation of T_c and *c*/*a* is investigated in NbB_2 and MoB_2-based superconducting diborides, which have totally different electronic structures mainly composed of *d* electron from transition metal. Our high-pressure electrical transport measurements and structural analysis reveal that the common positive correlation between T_c and *c*/*a* is observed in NbB_2, Zr-stabilized MoB_2, and these defected systems. Our insight opens further issues for the development of superconducting metal diborides.

I. INTRODUCTION

Exploration of superconductors attracts significant attention in materials composed of light elements with high Debye frequency, which is a constant of proportionality for superconducting critical temperature (T_c) within Bardeen-Cooper-Schrieffer (BCS) theory [1]. Among the explorations, high-T_c above 39 K have been discovered in MgB_2 crystallizing in AlB_2-type hexagonal structure (*P6*/*mmm*) about two decades ago [2]. Exploration of superconductivity in diborides with another transition metal (TM) except for MgB_2 is also continued to realize higher T_c [3–5]. However, all the examined TMB_2s exhibit drastically lower T_c than that of MgB_2. In a recent report, MoB_2 with $CaSi_2$-type rhombohedral structure (*R*-3*m*) shows a structural phase transition to the AlB_2-type at high pressure of 70 GPa and the second highest T_c of 32.4 K among superconducting TMB_2s is observed at 110 GPa [6]. The T_c monotonically increases with pressure above 100 GPa at a rate of 0.1 K/GPa and still does not show the trend of saturation. After the discovery, pressure-induced superconductivity in WB_2 with T_c of 17 K at 90 GPa has been immediately reported [7]. Also, the application of pressure suppresses antiferromagnetic transition in CrB_2 and induces superconductivity at 7 K under 110 GPa [8]. The high-pressure research opens a novel strategy to create high-T_c superconducting TMB_2s in the past few years.

The high T_c in MgB_2 originates from the strong coupling between σ-bands and E_{2g} phonon modes, which are related to the in-plane B–B bond. Based on the strong anisotropic feature, the *c*/*a*, known as a stretched *c*-lattice parameter, is an important character in superconducting metal borides. The relatively high *c*/*a* of 1.14 in MgB_2 contributes to the realization of high-T_c with a two-dimensional character [9,10]. In contrast, double sharp peaks of electronic density of state (DOS) at Fermi energy (E_F) in pressure-stabilized MoB_2, which are mainly composed of Mo d_z^2 orbital, provide high T_c above 30 K by coupling with out-of-plane vibrations in Mo [11]. In such the *d* electron system among TMB_2, the relationship between T_c and *c*/*a* is still uninvestigated issue for further exploration of high-T_c superconductors.

In this study, we investigate the relationship between T_c and *c*/a in superconducting TMB_2s via a high-pressure application, which is an effective way to manipulate the crystal structure without chemical modification. We select NbB_2, $Mo_{1-x}Zr_xB_2$, and these defected system $Nb_{1-x}B_2$ and $(Mo_{1-x}Zr_x)_{1-y}B_2$ as the candidates of examined AlB_2-type TMB_2s because these exhibit superconductivity at ambient pressure with *d* electron character [12,13]. The electrical transport properties and crystal structures in these materials under high pressure are measured to reveal the relationship between T_c and *c*/*a*. The T_c of NbB_2 is increased from 1.3 K to 9.2 K by introducing Nb deficiency [14]. Although the high-pressure study on superconductivity has been reported in the $Nb_{1-x}B_2$, the applied pressure is less than 6 GPa [15]. Also, a slight substitution of Zr in the Mo site stabilizes the metastable AlB_2-type structure in MoB_2 even at ambient pressure [13]. The $Mo_{1-x}Zr_xB_2$ and defected $(Mo_{1-x}Zr_x)_{1-y}B_2$ show superconductivity at 5.9 and 8.2 K, respectively [13]. Considering the drastic enhancement of T_c against pressure in the pressure-induced superconducting phase of pristine MoB_2, high-pressure behavior in the Zr-stabilized MoB_2 is also worth investigating. Our high-pressure electrical measurements and structural analysis suggest a positive relationship between T_c and *c*/*a* for all the examined TMB_2. The serial investigation of high-pressure behavior in TMB_2 is

helpful for further research on the exploration of superconductors in this system.

II. EXPERIMENTAL PROCEDURES

Polycrystalline samples of NbB_2, $Mo_{1-x}Zr_xB_2$, and $(Mo_{1-x}Zr_x)_{1-y}B_2$ were synthesized via argon arc-melting process. The starting materials with a stoichiometric composition ($x = 0.04$, $y = 0.15$) were placed on a water-cooled copper hearth in the furnace under an Ar atmosphere and melted several times to obtain a homogeneous sample. Defected $Nb_{1-x}B_2$ was synthesized by a solid-state reaction using a high-temperature and high-pressure method in a Kawai-type multi-anvil apparatus. A mixture of starting materials with a composition of Nb : B = 0.8 : 2 was filled into a sintered hexagonal BN tube. The prepared tube was compressed under 5 GPa and heated at 1200 ℃ for 0.5 h and quenched to room temperature. The details of sample preparation in the defected $Nb_{1-x}B_2$ are described in another paper [14].

The crystal structures of the obtained metal diborides at ambient pressure were confirmed by powder X-ray diffraction (XRD) analysis using a Mini Flex 600 (Rigaku) with Cu Kα radiation (λ = 1.5418 Å). In-situ XRD measurements were performed to reveal the crystal structure under high pressure for NbB_2, $Nb_{1-x}B_2$, $Mo_{1-x}Zr_xB_2$, and $(Mo_{1-x}Zr_x)_{1-y}B_2$ in diamond anvil cell (DAC) using synchrotron radiation at the AR-NE1A beamline of the Photon Factory (PF) at the High Energy Accelerator Research Organization (KEK). The X-ray beam was monochromatized to an energy of 30 keV (λ = 0.4180 Å for NbB_2 and $Nb_{1-x}B_2$, λ = 0.4172 Å for $Mo_{1-x}Zr_xB_2$ and $(Mo_{1-x}Zr_x)_{1-y}B_2$) and introduced through a collimator with a 50 μm diameter. One-dimensional XRD patterns were obtained from the collected Debye-Scherrer diffraction rings using the IPAnalyzer [16]. Re sheet with a 200 μm diameter hole was used as a gasket in DAC. The pulverized sample itself, or cubic BN, was filled in the hole of the gasket as the pressure-transmitting medium. Here, the XRD patterns of NbB_2 and $Nb_{1-x}B_2$ at ambient pressure were measured in DAC without compression. The results of XRD analysis under ambient pressure and high pressure are shown in Fig. S1 and S2.

The temperature dependence of the electrical resistance under high pressure in all the samples was measured via a four-probe method using the DAC with boron-doped diamond electrodes [17–19]. A stainless steel (SUS316) sheet with a 200 μm diameter hole was used for a gasket. Cubic BN powders were filled around the gasket hole, which act as the pressure-transmitting medium and an insulating layer between a gasket and the electrodes. Applied pressures in the DAC were estimated by the peak shift of a ruby fluorescence from a tiny piece of ruby in a sample space [20] and a Raman spectrum of diamond anvil [21] in both XRD analysis and electrical measurements.

III. RESULTS and discussion

The XRD analysis reveals that the synthesized samples exhibit an AlB_2-type structure (hexagonal, *P6*/*mmm*) at ambient pressure. The details, including the lattice constants, are shown in Fig. S1. The average amount of Nb deficiency x in $Nb_{1-x}B_2$ is determined to be 0.07 by comparing the lattice constant with that in the literature [14]. By using a similar estimation, the average amount of substituted Zr (x) in $Mo_{1-x}Zr_xB_2$ is determined to be 0.04 [13]. When the Zr amount x in $(Mo_{1-x}Zr_x)_{1-y}B_2$ is assumed to be 0.04, the amount of deficiency y is determined to be 0.1 from the reported relationship [13]. Hereafter, the compositions in these TMB_2 are written with the

aforementioned values, although a precise analysis of the composition is needed in future investigations.

Figure 1 (a-d) shows temperature (T) dependence of resistance (R) under various pressures at around low-temperature regions in NbB_2, $Nb_{0.93}B_2$, $Mo_{0.96}Zr_{0.04}B_2$, and $(Mo_{0.96}Zr_{0.04})_{0.90}B_2$. In the R-T curve of NbB_2 at the lowest pressure of 0.2 GPa, the resistance starts to decrease at 2.3 K, indicating superconductivity. The T_c, defined by the onset temperature of decreasing resistance, gradually decreases from 2.3 to 2.0 K with increasing pressure up to 34 GPa. The T_c near ambient pressure is drastically increased by introducing Nb deficiency, as shown in the R-T properties in $Nb_{0.93}B_2$. The T_c^{onset} of 7.7 K at 3 GPa monotonically decreases to 4.1 K at 39 GPa. The R-T curve of $Mo_{0.96}Zr_{0.04}B_2$ near ambient pressure shows a slight increase in resistance just above T_c, which is typically observed in nonhomogeneous superconductors with different transition temperatures [22]. This observation indicates a distributed Zr amount in synthesized $Mo_{0.96}Zr_{0.04}B_2$. The onset T_c of starting temperature of the reduction in resistance, which reflects the highest T_c in the inhomogeneous superconductor, decreases from 5.5K at ambient pressure to 3.7 K at 35 GPa. The T_c near ambient pressure in $(Mo_{0.96}Zr_{0.04})_{0.90}B_2$ is also enhanced by introducing the deficiency of $(Mo_{0.96}Zr_{0.04})$. The R-T behavior exhibits similar inhomogeneity, and T_c^{onset} gradually decreases from 8.0 K at 0.4 GPa to 6.0 K at 40 GPa. The inhomogeneity of superconducting transition in Zr-stabilized MoB_2 would be due to a distribution of the amount of deficiency and substitution. Also, a distortion in crystal, which is generally introduced during the arc-melting method, affects the sharpness of the superconducting transition [23]. The distortion will be improved by a post-annealing treatment after the arc-melting method [24]. Since the superconducting transition in all high-pressure measurements is broad due to the influence of a solid pressure-transmitting medium, the T_c values are determined using various criteria and exhibit a similar trend, as shown in Fig. S4. This suggests that the reduction in T_c is an intrinsic property of these compounds. In particular, the determination of T_c^{onset} in Zr-stabilized MoB_2 is presented in Fig. S5, as it is difficult to see. Also, all the samples maintain the metallic behavior even under high pressure, as shown in Fig. S2. Moreover, we examined an emergence of pressure-induced superconductivity in other metal diborides of AlB_2, TiB_2, ZrB_2, and VB_2, as shown in Fig. S3. No superconductivity is observed in these diborides at least less than 50 GPa. In this study, all the evaluations for superconductivity are performed via the electrical transport measurements, which reflect the local properties in the DAC with large pressure distribution. For future research, temperature-dependent magnetization measurements under high pressure could reveal bulk superconducting properties and provide deeper insights into the underlying physics of this system.

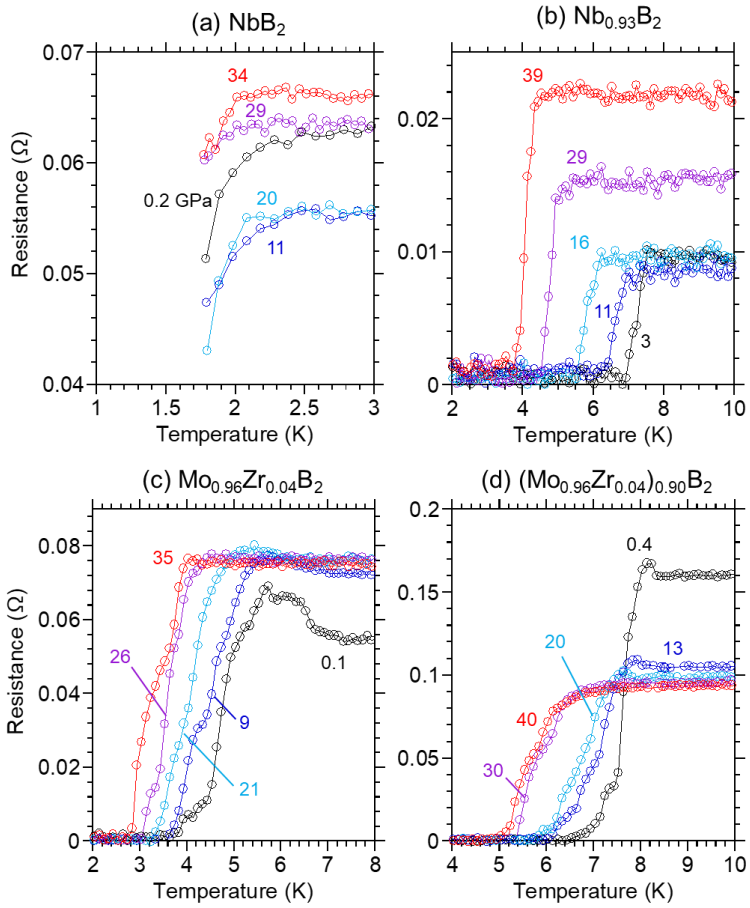

FIG. 1. Temperature dependence of resistance at around low-temperature region in all the obtained samples under high pressure. (a) NbB_2, (b) $Nb_{0.93}B_2$, (c) $Mo_{0.96}Zr_{0.04}B_2$ and (d) $(Mo_{0.96}Zr_{0.04})_{0.90}B_2$.

Figure 2 (a) shows a pressure dependence of T_c in NbB_2 and $Nb_{0.93}B_2$ up to around 40 GPa. The T_cs linearly decrease as a function of the pressure with the slope of $dT_c/dP = -0.012$ K/GPa in NbB_2 and -0.086 K/GPa in $Nb_{1-x}B_2$. Compared with $dT_c/dP = -1.11$ K/GPa in MgB_2 [25], NbB_2 and $Nb_{0.93}B_2$ have blurry pressure-dependence of T_c. The high-pressure effect on T_c in MgB_2 has been understood within the range of a conventional BCS-type superconductor. The T_c is drastically reduced by pressure due to a decrease in DOS at E_F and an increase in averaged phonon frequency, reducing electron-phonon coupling strength [26,27]. The negative correlations in NbB_2 and $Nb_{0.93}B_2$ are also understood to be the same as the case of MgB_2. A smaller phonon frequency in NbB_2 possibly contributes to exhibiting the blurry change in T_c as a function of pressure [28]. Also, the amount of Nb deficiency x in $Nb_{1-x}B_2$ is estimated to be 0.11 from the comparison between the intercept of dT_c/dP and the reported value [15], which is larger than that estimated by XRD analysis. Figure 2 (b) shows a pressure-dependent T_c in $Mo_{0.96}Zr_{0.04}B_2$ and $(Mo_{0.96}Zr_{0.04})_{0.90}B_2$. Although a positive correlation of T_c against pressure is expected as the behavior in pressure-stabilized AlB_2-type MoB_2 [6], the T_c in both Zr-stabilized MoB_2s exhibit negative slopes with $dT_c/dP = -0.054$ K/GPa in $Mo_{0.96}Zr_{0.04}B_2$ and -0.045 K/GPa in $(Mo_{0.96}Zr_{0.04})_{0.90}B_2$. Yet, the positive slope of T_c in MoB_2 at high pressure deviates from theoretical calculations, suggesting the negative correlation due to the reduction of DOS at E_F and phonon hardening [28]. Also, a steady decrease of T_c from 8 K at 0 GPa to 4 K at 50 GPa in Nb-

stabilized MoB_2 has recently been reported in a high-pressure experiment [29]. Our observations of T_c reduction in Zr-stabilized MoB_2s show a similar trend as their research.

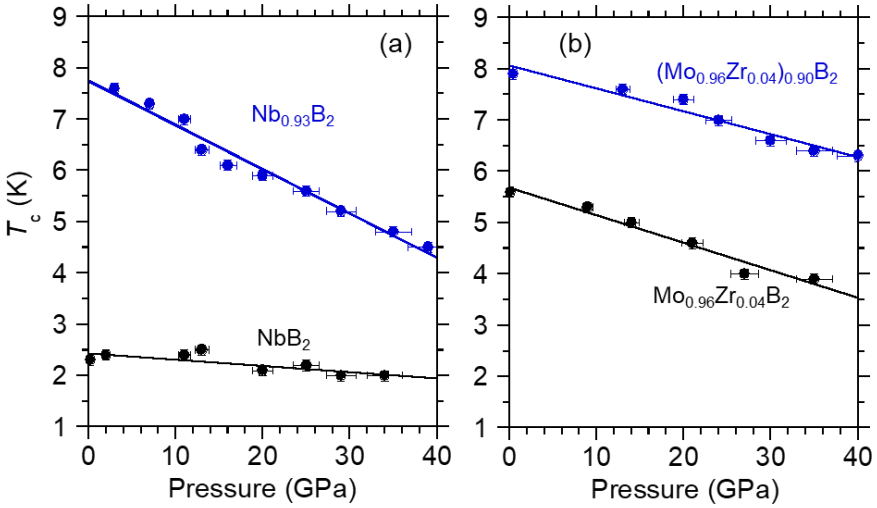

FIG. 2. (a) Applied pressure dependence of T_c of NbB_2 and $Nb_{0.93}B_2$, (b) $Mo_{0.96}Zr_{0.04}B_2$, and $(Mo_{0.96}Zr_{0.04})_{1-y}B_2$.

To investigate the relationship between superconducting properties and crystal structure, XRD patterns were measured under various pressures, as shown in Fig. 3. The AlB_2-type structures of all the samples are maintained at around 30 GPa without a structural phase transition. Figure 4 (a) and (b) shows the pressure dependences of lattice constants a and c in NbB_2, $Nb_{0.93}B_2$, $Mo_{0.96}Zr_{0.04}B_2$, and $(Mo_{0.96}Zr_{0.04})_{0.90}B_2$, which are determined from the peak position in XRD patterns. The lattice constants of all the compounds monotonically decrease with increasing pressure. The stretched c-lattice parameter c/a of these compounds is plotted as a function of pressure in Fig. 4 (c). The decreasing rate of c/a in $Nb_{0.93}B_2$ (-2.2×10^{-4} GPa^{-1}) is higher than that in NbB_2 (-1.2×10^{-4} GPa^{-1}). A similar tendency is observed in stabilized MoB_2, namely, the decreasing rate of c/a in $(Mo_{0.96}Zr_{0.04})_{0.90}B_2$ is -6.4×10^{-4} GPa^{-1}, which is almost twice, compared with that of -2.7×10^{-4} GPa^{-1} in $Mo_{0.96}Zr_{0.04}B_2$. These results suggest that the defected system in TMB_2 has the common feature of sensitive c/a against applied pressure. Also, the pressure dependence of T_c and c/a exhibits a similar trend with a negative correlation in all the examined superconducting TMB_2.

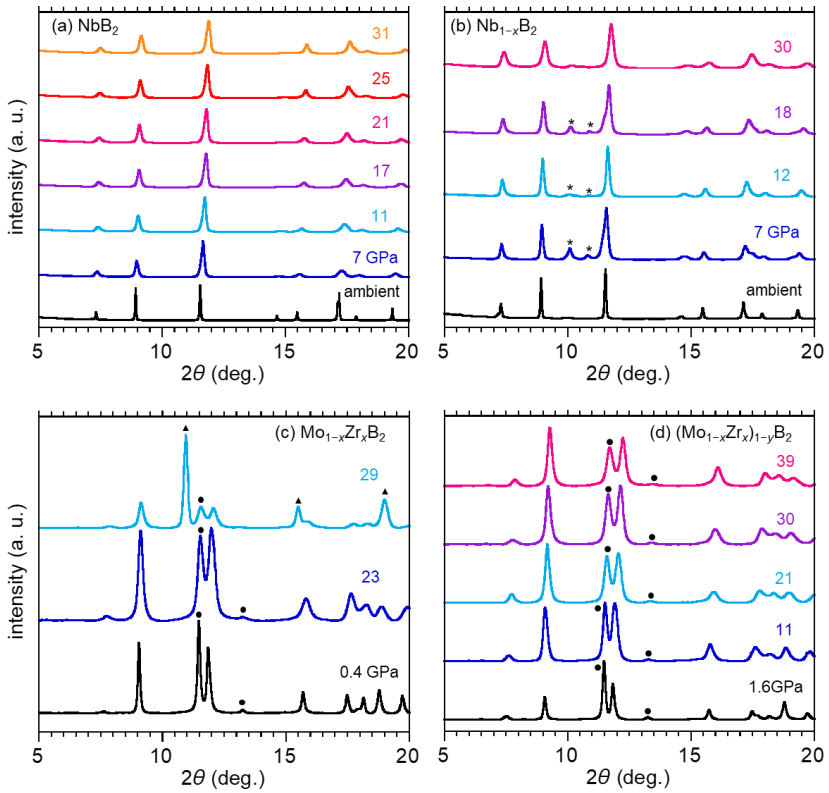

FIG. 3. XRD pattern under high pressure of (a) NbB_2, (b) $Nb_{1-x}B_2$, (c) $Mo_{1-x}Zr_xB_2$, and (d) $(Mo_{1-x}Zr_x)_{1-y}B_2$.

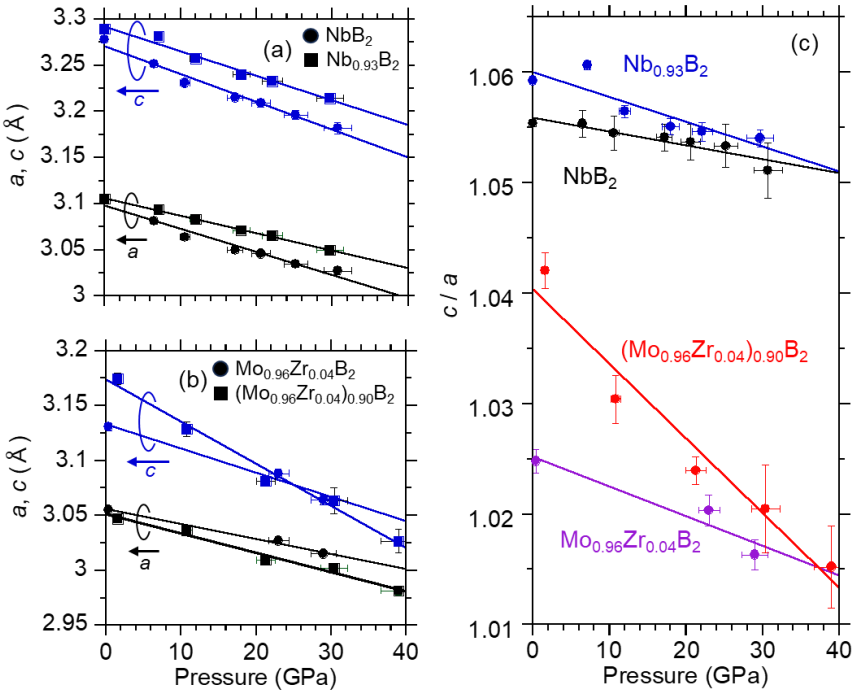

FIG. 4. Pressure-dependent lattice constants *a* and *c* in (a) NbB_2 and $Nb_{0.93}B_2$, (b) $Mo_{0.96}Zr_{0.04}B_2$ and $(Mo_{0.96}Zr_{0.04})_{0.90}B_2$, and (c) The *c*/*a* in these compounds.

Finally, the relationship between *c*/*a* and T_c in NbB_2, $Nb_{0.93}B_2$, $Mo_{0.96}Zr_{0.04}B_2$, and $(Mo_{0.96}Zr_{0.04})_{0.90}B_2$ are shown in Fig. 5. Because experimentally observed *c*/*a* and T_c are measured under slightly different pressures, these values measured at nearest pressures are used for the circle plots. The straight lines are determined from the slopes in the pressure dependence of *c*/*a* and T_c.

Interestingly, a positive trend between T_c and c/a is commonly observed in the examined samples. This fact suggests that c/a is strongly correlated with superconductivity in NbB_2 and MoB_2 systems with a large contribution of d electron to E_F [12,13], in spite of different electronic states with MgB_2, which exhibit p electron feature [30]. In particular, the electronic structure in MoB_2-based systems is mainly composed of Mo dz^2 orbital, coupled with out-of-plane vibrations in Mo. This observation highlights the universal importance of two-dimensionality in the crystal structure for superconductivity in TMB_2, regardless of characteristics in electronic structure. A possible explanation for this correlation is the contribution of B p orbitals to E_F. In the NbB_2 system, the in-plane dispersion of σ-bonding in B 2p states contributes to E_F[12], despite the dominant Nb d orbital character. Similarly, in-plane breathing-like vibrations of B atoms are believed to enhance superconductivity in pristine MoB_2[6]. Additionally, high-T_c MoB_2, which exhibits the T_c of 32 K under extreme pressure, has a high c/a value of 1.09[11], comparable with that in MgB_2. Furthermore, the theoretically predicted AlB_2-type CaB_2 with the estimated T_c above 50 K at 30 GPa [31] is suggested to have the highest c/a of 1.27 among superconducting TMB_2. Although the obvious mechanism of this correlation is still an open question, the observed relationship between c/a and T_c provides valuable insights for further research on metal diborides.

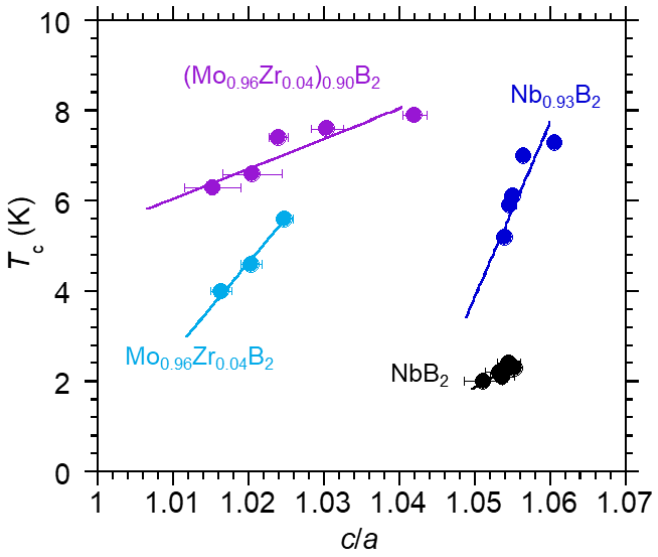

FIG. 5. Relationship between c/a and T_c in NbB_2, $Nb_{0.93}B_2$, $Mo_{0.96}Zr_{0.04}B_2$ and $(Mo_{0.96}Zr_{0.04})_{0.90}B_2$.

IV. CONCLUSIONS

The high-pressure electrical transport measurements and structural analysis for superconducting NbB_2, $Nb_{0.93}B_2$, $Mo_{0.96}Zr_{0.04}B_2$, and $(Mo_{0.96}Zr_{0.04})_{0.90}B_2$ reveal that the relationship between the T_c and a stretched c-lattice parameter (c/a), which is considered as important parameter for high-T_c superconductivity in MgB_2. All the examined diborides exhibit a common correlation in T_c and c/a with a positive slope. The observation makes an open issue for the guideline of development in superconducting diborides because the electronic state and key factor for superconductivity between MgB_2 and superconducting TMB_2 is totally different. The c/a is expected to be a future guideline for the exploration of high-T_c superconductors in metal diborides and related materials.

ACKNOWLEDGMENTS

This work was partly supported by JSPS KAKENHI Grant Number 23H01835, 23K13549, and 23KK0088. The fabrication process of diamond electrodes was partially supported by the NIMS Nanofabrication Platform in the Nanotechnology Platform Project sponsored by the Ministry of Education, Culture, Sports, Science and Technology (MEXT), Japan. The synchrotron X-ray experiments were performed at AR-NE1A (KEK-PF) under the approval of Proposal No. 2022G049 with support from Dr. Y. Shibazaki (KEK).

References

[1] Bardeen J, Cooper L N and Schrieffer J R 1957 Theory of Superconductivity *Phys. Rev.* **108** 1175–204

[2] Nagamatsu J, Nakagawa N, Muranaka T, Zenitani Y and Akimitsu J 2001 Superconductivity at 39 K in magnesium diboride *Nature* **410** 63–4

[3] Leyarovska L and Leyarovski E 1979 A search for superconductivity below 1 k in transition metal borides *Journal of the Less Common Metals* **67** 249–55

[4] Barbero N, Shiroka T, Delley B, Grant T, Machado A J S, Fisk Z, Ott H-R and Mesot J 2017 Doping-induced superconductivity of ZrB 2 and HfB 2 *Phys. Rev. B* **95** 094505

[5] Cooper A S, Corenzwit E, Longinotti L D, Matthias B T and Zachariasen W H 1970 Superconductivity: The Transition Temperature Peak Below Four Electrons per Atom *Proc. Natl. Acad. Sci. U.S.A.* **67** 313–9

[6] Pei C, Zhang J, Wang Q, Zhao Y, Gao L, Gong C, Tian S, Luo R, Li M, Yang W, Lu Z-Y, Lei H, Liu K and Qi Y 2023 Pressure-induced superconductivity at 32 K in MoB2 *National Science Review* **10** nwad034

[7] Lim J, Hire A C, Quan Y, Kim J S, Xie S R, Sinha S, Kumar R S, Popov D, Park C, Hemley R J, Vohra Y K, Hamlin J J, Hennig R G, Hirschfeld P J and Stewart G R 2022 Creating superconductivity in WB2 through pressure-induced metastable planar defects *Nat Commun* **13** 7901

[8] Pei C, Yang P, Gong C, Wang Q, Zhao Y, Chen K, Yin Q, Tian S, Li C, Cao W, Lei H, Cheng J and Qi Y Pressure-induced superconductivity in itinerant antiferromagnet CrB2

[9] Singh P P 2003 Electron–phonon interaction in NbB2: a comparison with MgB2 *Solid State Communications* **125** 323–6

[10] Wan X, Dong J, Weng H and Xing D Y 2001 Band structure of MgB2 with different lattice constants *Phys. Rev. B* **65**

[11] Liu X, Huang X, Song P, Wang C, Zhang L, Lv P, Liu L, Zhang W, Cho J-H and Jia Y 2022

Strong electron-phonon coupling superconductivity in compressed α − MoB 2 induced by double Van Hove singularities *Phys. Rev. B* **106** 064507

[12] Xiao R J, Li K Q, Yang H X, Che G C, Zhang H R, Ma C, Zhao Z X and Li J Q 2006 Correlations among superconductivity, structural instability, and band filling in Nb 1 − x B 2 at the critical point x ≈ 0.2 *Phys. Rev. B* **73** 224516

[13] Muzzy L E, Avdeev M, Lawes G, Haas M K, Zandbergen H W, Ramirez A P, Jorgensen J D and Cava R J 2002 Structure and superconductivity in Zr-stabilized, nonstoichiometric molybdenum diboride *Physica C: Superconductivity* **382** 153–65

[14] Yamamoto A, Takao C, Masui T, Izumi M and Tajima S 2002 High-pressure synthesis of superconducting Nb1−xB2 (x=0–0.48) with the maximum Tc=9.2 K *Physica C: Superconductivity* **383** 197–206

[15] Escamilla R, Lovera O, Akachi T, Durán A, Falconi R, Morales F and Escudero R 2004 Crystalline structure and the superconducting properties of NbB_{2+x} *J. Phys.: Condens. Matter* **16** 5979–90

[16] Seto Y, Hamane D, Nagai T and Fujino K 2008 Fate of carbonates within oceanic plates subducted to the lower mantle, and a possible mechanism of diamond formation *Phys Chem Minerals* **35** 223–9

[17] Matsumoto R, Sasama Y, Fujioka M, Irifune T, Tanaka M, Yamaguchi T, Takeya H and Takano Y 2016 Note: Novel diamond anvil cell for electrical measurements using boron-doped metallic diamond electrodes *Review of Scientific Instruments* **87** 076103

[18] Matsumoto R, Irifune T, Tanaka M, Takeya H and Takano Y 2017 Diamond anvil cell using metallic diamond electrodes *Jpn. J. Appl. Phys.* **56** 05FC01

[19] Matsumoto R, Yamashita A, Hara H, Irifune T, Adachi S, Takeya H and Takano Y 2018 Diamond anvil cells using boron-doped diamond electrodes covered with undoped diamond insulating layer *Appl. Phys. Express* **11** 053101

[20] Mao H K, Bell P M, Shaner J W and Steinberg D J 1978 Specific volume measurements of Cu, Mo, Pd, and Ag and calibration of the ruby R1 fluorescence pressure gauge from 0.06 to 1 Mbar *Journal of Applied Physics* **49** 3276–83

[21] Akahama Y and Kawamura H 2004 High-pressure Raman spectroscopy of diamond anvils to 250GPa: Method for pressure determination in the multimegabar pressure range *Journal of Applied Physics* **96** 3748–51

[22] Zhang G, Zeleznik M, Vanacken J, May P W and Moshchalkov V V 2013 Metal–Bosonic Insulator–Superconductor Transition in Boron-Doped Granular Diamond *Phys. Rev. Lett.* **110** 077001

[23] Sobczak Z, Winiarski M J, Xie W, Cava R J and Klimczuk T 2019 Superconductivity in the intermetallic compound Zr_5Al_4 *EPL* **127** 37005

[24] Yuan L, Wang W, Li Y, Yang M, Zhang H and Zhang W 2020 Effect of annealing temperature on texture and residual stress of Ti-6Al-4V alloy seamless tubing processed by cold rotary swaging *Vacuum* **177** 109399

[25] Deemyad S, Schilling J S, Jorgensen J D and Hinks D G 2001 Dependence of the superconducting transition temperature of MgB2 on pressure to 20 GPa *Physica C: Superconductivity* **361** 227–33

[26] Zhang C and Zhang X 2011 Effect of negative pressure on superconducting transition temperature of MgB2 *Computational Materials Science* **50** 1097–101

[27] Loa I and Syassen K 2001 Calculated elastic and electronic properties of MgB2 at high pressures *Solid State Communications* **118** 279–82

[28] Carmona-Galván M-A, Heid R and Peña-Seaman O D la 2023 Electron-phonon coupling and superconductivity in $α$-MoB$_2$ as a function of pressure *Phys. Scr.* **98** 115975

[29] Lim J, Sinha S, Hire A C, Kim J S, Dee P M, Kumar R S, Popov D, Hemley R J, Hennig R G, Hirschfeld P J, Stewart G R and Hamlin J J 2023 Niobium substitution suppresses the superconducting critical temperature of pressurized MoB 2 *Phys. Rev. B* **108** 094501

[30] Morshedloo T, Roknabadi M R and Behdani M 2015 First-principles study of the superconductivity in MgB2 bulk and in its bilayer thin film based on electron–phonon coupling *Physica C: Superconductivity and its Applications* **509** 1–4

[31] Choi H J, Louie S G and Cohen M L 2009 Prediction of superconducting properties of CaB 2 using anisotropic Eliashberg theory *Phys. Rev. B* **80** 064503